3-D Electrical Resistivity Imaging with Compressive Sensing: Application to Simulate Soil-Water-Disease Interactions of Citrus Trees

Shashi Ranjan

A Thesis Submitted to
Indian Institute of Technology Hyderabad
In Partial Fulfillment of the Requirements for
The Degree of Master of Technology

भारतीय प्रौद्योगिकी संस्थान हैदराबाद
Indian Institute of Technology Hyderabad

Department of Civil Engineering

July 2016

Declaration

I declare that this written submission represents my ideas in my own words, and where ideas or words of others have been included, I have adequately cited and referenced the original sources. I also declare that I have adhered to all principles of academic honesty and integrity and have not misrepresented or fabricated or falsified any idea/data/fact/source in my submission. I understand that any violation of the above will be a cause for disciplinary action by the Institute and can also evoke penal action from the sources that have thus not been properly cited, or from whom proper permission has not been taken when needed.

Shashi Ranjan

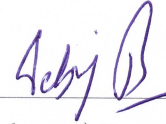(Signature)

SHASHI RANJAN

(Shashi Ranjan)

CE14MTECH11024

(Roll No.)

Approval Sheet

This Thesis entitled 3-D Electrical Resistivity Imaging with Compressive Sensing: Application to Simulate Soil-Water-Disease Interactions of Citrus Trees by Shashi Ranjan is approved for the degree of Master of Technology from IIT Hyderabad

(Dr. Bhabani S. Mallik) Examiner
Dept. of Chemistry
IITH

(Dr. Debraj Bhattacharyya) Examiner
Dept. of Civil Engg
IITH

(Dr. K.B.V.N. Phanindra) Adviser
Dept. of Civil Engg
IITH

Acknowledgements

This dissertation would not have been possible without the guidance and help of several individuals who in one way or another have contributed and extended their valuable assistance in the preparation and completion of this study.

First and foremost, I would like to convey my sincerest gratitude to Dr. K B V N Phanindra for his guidance and supervision throughout the tenure of this project. It was his encouragement, co-operation and support that has helped in the successful completion of this dissertation.

I shall be thankful to Dr. B. Umashankar (Assistant Professors, Department of Civil Engineering, IIT Hyderabad) and Dr. C.S. Sastry (Assistant Professors, Department of Mathematics, IIT Hyderabad) for their support in completion of the project.

I would also like to acknowledge the contribution of Mr. Srinivasa Rao , Mr. Prasad Theeda and Mr. Pradeep (Research Scholars), who helped me throughout the project.

I extend my gratitude to all my friends especially Ankit Deshmukh, Chillara Reddy Varaprasad, Surjeet Rawat for their kind and timely co-operation in all aspects for the completion of this dissertation.

Last but not the least, I would like to owe my deepest gratitude to my parents and family members whose love and blessings have been a constant source of motivation and strength.

Dedication

I dedicate this to my mother and father

Abstract

This research is organized into two parts. First part of the work aims at understanding the inversion mechanism of electrical resistivity tomography (ERT) from first principles. A compressive sensing (CS) based ERT inversion algorithm was developed for use with sub-surface image reconstruction. Second part of the research aims at developing efficient irrigation water management scenarios considering health of the citrus tree using experimental and numerical studies.

Geophysical techniques are widely used to characterize hydrological fluxes that are controlling sub-surface dynamics. Of these, ERT has proven to be the prominent and robust technologies for imaging the sub-surface. The strength of a geophysical inversion technique to reconstruct the image is largely dependent on the strategy adopted to solve the ill-posed, under-determined, non-linear system. Conventional gradient based algorithms that use Euclidean norm minimization with some sort of regularization may fail to detect the sharp interfaces between earth layers and resistivity anomalies. Given the fact that, earth's resistivity (and hence, hydro-geologic) features varies abruptly on a continuous spatial domain; the sparsity in model parameter change can be better utilized to apply CS algorithms for resistivity imaging. CS based 3-D image reconstruction algorithms from ERT observations were not reported in literature till date.

We developed an open-source, 3-D MATLAB code to invert static ERT data using CS algorithm. Primal-dual interior point method was used as CS algorithm to solve large scaled L1-regularized least square problem. Preconditioned conjugate gradient algorithm was used to compute search direction. Discrete cosine transform has been applied as the orthogonal matrix to sparsely represent the change in model parameters. The developed code was tested on two synthetic models having parameter sparsity in radial and depth directions. Results of the inversion technique conclude that; CS is able to capture the sub-surface electrical properties far better than gradient algorithms (Normalized RMSE of 0.467 after 10 iterations from Gauss-Newton

algorithm against 0.786 after 5 iterations from CS algorithm). In particular, when the model parameters are increased through refinement (satisfying the inherent condition on sparsity), CS is able to perfectly capture the resistivity distribution.

In the second part of the research, we aimed at understanding soil-water-disease interactions of Citrus trees situated in a semi-arid tropical agro-climatic condition. Such interactions can help in developing spatial-temporal patterns of root water up-take (RWU) in relation to the health of the tree, so that farmers can efficiently manage the available water resources. Two experimental plots, one around a healthy-matured and other around a declined-matured citrus tree in Vidarbha region of Maharashtra were considered for our analysis.

A 3-D ERT setup consisting of 40 surface electrodes placed in dipole-dipole configuration on a grid of 2.8 x 2.8 m with orange tree at the center was developed to monitor sub-soil dynamics in response to irrigation and RWU. Laboratory estimation of soil moisture and electrical conductivity for soils of different horizons were done following ASTM guidelines to develop pedo-electric relations considering modified Archie's law parameters. Healthy and declined citrus trees have shown clearly distinct soil moisture profiles following irrigation. This made us to revisit the parameters controlling root distribution using a numerical framework.

3-Dimensional form of Richards equation was numerically solved using HYDRUS-2D/3D for the two sites to generate soil moisture and RWU profiles. Care was taken to match the node locations between ERT and HYDRUS grids, for ease with calibration. Soil-atmospheric fluxes were provided using estimated evaporation and transpiration rates, following FAO guidelines. Water leaving the model was estimated using Darcy's law with gradient calculated from the tensiometer placed at different depths below the root zone. Soil water retention and un-saturated hydraulic conductivity functional parameters were estimated using van Genuchten Mualem constitutive relationships. One at a time sensitivity analysis is performed in both cases, to arrive at the optimal parameters controlling RWU. Optimal root distribution parameters were differed

marginally between healthy and declined trees. Also, RWU (averaged for the model domain) of a declined citrus tree is significantly less to that of a healthy tree with delayed peaks. This concludes that, water stress resulting from the health of a tree (in spatio-temporal domain) has to be accounted in RWU simulation models. The calibrated model can be used to develop soil moisture and RWU patterns of healthy and declined citrus trees for implementing management scenarios.

Contents

Chapter 1

Introduction

1.1 Introduction

In every modelling technique, inversion problem has been used knowingly or unknowingly. In 3D ERT modelling , one has to deal with under-determinate, ill-posed, Non-linear problem which generally includes huge matrices during calculation. Non-linearity exist in the model due to the measurement technique we uses to obtain the data. There are no inversion tool available for non-linear problem and it has been solved by first linearizing the problem and using the inversion technique available for linear problems. Ill-posed condition of the problem exist due to discontinuous forward operator of ERT problem, which leads to non-convergence of the solution. Some kind of regularization technique has been sought to give better convergence. Another thing is highly under-determined problem of ERT which leads to non-uniqueness of the solution and solved by using a-priori information about the model. A efficient inversion tool is always compulsory for better results and for better model. There

are very few open source, platform independent inversion packages available for 3D ERT modelling. A fast inversion technique is also required to handle big matrices and computationally inexpensive so that one could work on computers having standard specifications. Most of the inversion packages available for ERT are gradient based and uses l2-norm minimization which ultimately gives smooth images after inversion. Main drawback of this technique is its inability to detect sharp changes in resistivity structure. Gradient based method generally requires a-priori information about model to converge effectively otherwise it may diverge or may not converge at all. On the other hand, Compressed sensing theory states that it can reconstruct the model with a fewer data points than general inversion technique. It generally uses l1-norm regularization which can detect sharp transition in resistivity more effectively. But compressed sensing technique can be only used when model has sparsity on some orthonormal basis which we have to explore in case of ERT.

Globally, India ranks third in orange production, accounting for 7.60% of worlds tonnage [1]. However, India ranks 64th in orange crop productivity (yield per unit area), accounting for 9.23 tons/ha. Orange crop productivity in India is far behind many developed and developing countries. Vidarbha region in Maharashtra, India is the leading Mandarin orange (Citrus reticulata) producing region in the country accounting for 40 % of Country's production with a yield of 6 tons/ha, far below the nations average [1]. The main cause of this low productivity is bacteria called Phytopthora spp. which cause water mold disease like Gummosis and root rot. Till date, significant amount of research has been done on chemical and biological treatment of these disease but no significant research has been published in understanding the mechanisms by which, disease causing pathogens can alter soil-water-plant relations within the rhizosphere of citrus orchards. So in this study, an attempt has been made to simulate soil-water-plant interaction using field and laboratory setups to get necessary parameters and ultimately solve the water flow equation.

1.2 Objective of the research

There are two main objectives of this work:

1.2.1 Comparing various inversion algorithms

Our main objective in this section of the study is to develop an open source MATLAB based 3D resistivity inversion package using Compressed Sensing. It includes following tasks:

1. Linearization of Non-linear Inversion problem of ERT.

2. Formulation of Sensitivity (Jacobian) matrix.

3. Provision of Sparsity using discrete Cosine Transformation into the model.

4. Comparison of inversion results using Compressed Sensing with that of Gradient methods.

5. Comparison of Inversion results under various scenarios using synthetic model.

1.2.2 Modeling soil water-disease interaction of orange trees

In this section, our main objective will be to Simulate Soil-Water-Disease interaction using HYDRUS. It includes following tasks:

1. Development and validation of 3D ERT Protocols (dipole-dipole and multi-gradient) for the measurement.

2. Laboratory measurement of soil properties.

3. Development of moisture content and resistivity relationship (Archie's law parameters).

4. Development of Soil-water characteristic curve.

5. Optimization of root water uptake parameter using HYDRUS.

1.3 Literature Review

The inverse problem in resistivity interpretation was described first when Slichter reported a method of interpretation of resistivity data over a layered earth using Hankel's Fourier-Bessel inversion formula [2]. It gives a unique solution if the resistivity is a continuous function of electrode spacing. In practice, resistivity measurements are limited to a small number of readings taken at discrete electrode spacing. Thus a unique resistivity response does not exist [Constable et al., 1987.]. Vozoff used this method on field and synthetic data generated for three- and four-layer models [3]. Zohdy proposed a method of direct resistivity-interpretation which is valid for noisy data as well [4]. However, none of these earlier investigations deal with existence, uniqueness, construction and stability, which are important concerns and must be dealt with within any inverse problem. Backus and Gilbert introduced a linear inverse theory for geophysical problems [5]. They thoroughly discussed model resolution, least-squares fit of the data and solution uniqueness. The method is valid even for noisy or insufficient data, and they quantified the trade-off between resolution and stability for solutions to inverse problems. Following Backus and Gilberts work, generalized linear inverse theory was described by Jackson in terms of linear algebra ([6] [7]). Since the forward problem of electrical soundings for stratified media was solved by means of the linear filter theory many articles have appeared dealing with automatic and numerical interpretation [8]. This approach looks for a fit between the experimental and the theoretical data in a least squares sense, either in the resistivity transform domain or in the apparent resistivity domain. Different error functions have been proposed and different minimization procedures considered. In present time, most of the inversion tools/software uses gradient based algorithms like

steepest gradient, conjugate gradient, Gauss-Newton, etc. which gives very good results. In recent times due to increase in computational capacity a number of iterative optimization methods have been used. Even then due to non-linearity of inversion problem, problem doesn't converge many times. So giving a-priori information of the model in the inversion technique and using regularization technique, it is easier to get the solution. In the inversion problem, solution would be extremely unstable and unrealistic and to overcome these difficulties, regularization methods are applied.

Phytopthora spp. are the most destructive pathogens of citrus trees, causing soil and water borne diseases including root rot and gummosis [9]. These root pathogens can damage the tree by decreasing root density and water-nutrient uptake [10]. A significant loss of citrus production resulting from these pathogens has been reported in high rainfall subtropics of the world ([11], [12], [13]). Detection of Phytopthora spp. species is being done in a conventionally way, using microscopic examination of morphological characteristics, isolation of pathogen on culture media, and psychological traits (Das et. al., 2011). Disease management of Phytopthora spp. includes use of tolerant root stocks, fungicides, and biological controls [14]. The use of chemical fungicides can result in increased degree of pathogen resistance ([15] [16]). Application of Eco-friendly treatments like bio-agents and botanicals from natural plant extracts can be thought of a viable alternative for treating disease causing pathogens [12]. A significant amount of research has been done across the world on chemical and biological treatment of phytopthora spp. affected citrus trees, with less attention given to understand the root water uptake mechanism caused by disease causing pathogens. Till date, no significant research has been published in understanding the mechanisms by which, disease causing pathogens can alter soil-water-plant relations within the rhizosphere of citrus orchards. One reason for this include management and control of Phytopthora in citrus trees is largely viewed from pathology and molecular biology disciplines rather than agronomy and hydrology ([17], [18],[16], [14], [12], [13]). Bright and Graham (2004) [13] have studied the effect of soil, rootstock and

climatic parameters on phytopthora spp. population growth, and concluded that, molecular biology and water-holding capacity of fine textured soils have a profound effect on the growth of disease causing bacteria.

1.4   Organization of thesis

The thesis is organized into FIVE chapters which is as follows:

Chapter one is basically the introduction of the whole study. It contains motivation behind the study in the sub-introduction followed by objectives of the study, and the literature reviews on the study topic are provided at the end.

Chapter two first covers the theory behind 3D forward and inversion problem. Then various gradient based algorithm are discussed. compressed sensing theory and algorithm are discussed later in this part. At the end of chapter, we have explained the matlab implementation technique used followed by development and use of synthetic problem used in the study.

Chapter three explains the theory behind modelling technique used in soil-water-disease simulation. In this part, we have discussed field and laboratory experimental setups and methodology adopted during the experimentation. Simulation of water flow using Richard's equation has been explained later in this part.

Comparison of results of the 3D ERT inversion using various algorithm has been provided and discussed in chapter four. Results from simulation of soil-water-plant interaction has been also discussed later in this chapter.

Summary and conclusions, followed by future scope and limitation of the study was presented in Chapter Five.

Chapter 2

A MATLAB based Resistivity Inversion Model

2.1 FORWARD MODELING

The (mathematical) process of predicting data based on some physical or mathematical model with a given set of model parameters (and perhaps some other appropriate information, such as geometry, etc.). The forward problem solution makes it possible to predict geophysical data for specific geological structures. In this work, Singular value Decomposition has been used for calculating pseudo-inverse of forward operator to calculate the data based on given model parameters.

model {model parameters 's', sources 's'} = data {'d'}

$$d = A(m) \qquad (2.1)$$

where A is the forward problem operator depending on a source s.

The procedure of forward modelling is defined by Meju [19] that "given some information on the values of sets of parameters (no. of layers, resistivity, thickness of layers) for a hypothetical earth model, a theoretical relationship (mathematical model) is used to derive the values of some measurable quantities (apparent resistivity, phases)".

2.1.1   Governing Equation

DC resistivity and electrical resistivity tomography experiments yield a series of voltage measurements in response to a series of known input currents. These voltages and currents are related to the subsurface conductivity structure via the following relationship:

$$\nabla \cdot (-\sigma \nabla \phi) = I(\delta(r - r_{s+}) - \delta(r - r_{s-})) \tag{2.2}$$

Equation 2.2 is the partial differential equation that relates the potential field (ϕ) to the input current (I), from a dipole, through the conductivity structure of the medium (σ). Here, r_{s+} and r_{s-} are the locations of the positive and negative current sources, respectively, and $\delta(r - r_s)$ is the Dirac delta function, centered at the current source location. In matrix notation, according to Pidlisecky[20] we can write equation 2.2 as follows :

$$(D \cdot S(\sigma) \cdot G)u = A(\sigma)u = q \tag{2.3}$$

Here, D and G are matrices representing 3D divergence and gradient operators, respectively; $S(\sigma)$ is a diagonal matrix containing the conductivity values; u is a vector containing the potentials; $A(\sigma)$ is the complete forward operator matrix; and q is a vector containing the locations of the positive and negative current sources. From equation 2.3, we can calculate potentials for a given resistivity model using

following equation:

$$u = A^{-1}(\sigma)q \tag{2.4}$$

Since equation 2.4 will give potential everywhere in the 3D volume and data observed in the field are the subset of this potential, so a projection matrix Q has been defined for selecting the data points from the volume.

$$d = Qu = QA^{-1}(\sigma)q \tag{2.5}$$

from equation 2.5;We can clearly observe that relationship between data and model parameters are non-linear. So we can't write forward model in the following form:

$$d = G \cdot m \tag{2.6}$$

Non-linearity of forward model of electrical resistivity tomography has been illustrated in Meju (1994) [19] using Wenner configuration on a 2D model.
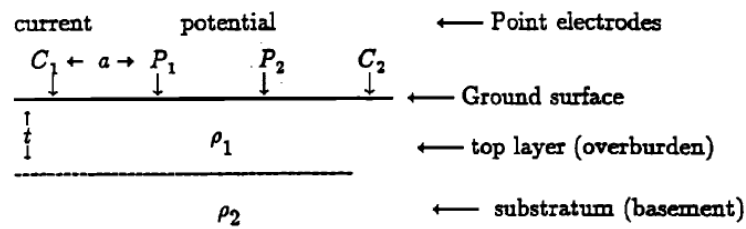
Figure 2.1: 2D model used by Meju

The forward theory states that the apparent resistivity observable on the surface of the above hypothetical earth model is given by:

$$\rho_a = \rho_1(1 + 4\sum_{(n=1)}^{\infty} k^n/\sqrt{[1 + (2nt/a)^2]} - 2\sum_{(n=1)}^{\infty} k^n/\sqrt{[1 + (nt/a)^2]}) \qquad (2.7)$$

where;

$$k = (\frac{\rho_2 - \rho_1}{\rho_2 + \rho_1}) \qquad (2.8)$$

where k is the reflection coefficient at the interface between the top layer and the basement. On examination of above equation is reveals that we can't perform a simple linearizing parameterization for resistivity problem.

2.2 INVERSE MODELING

Meju (1994) [19] described the inverse procedures as: 'Given some information on the values of some measured quantities (field or experimental data), we use a theoretical relationship to derive the values of the set of parameters that explains or reproduces our field observations. Inverse theory is the fine art of estimating model parameters from data. It requires a knowledge of the forward model capable of predicting data if the model parameters were, in fact, already known. Anyone who attempts to solve a problem in the sciences is probably using inverse theory, whether or not he or she is aware of it. Inverse theory, however, is capable (at least when properly applied) of doing much more than just estimating model parameters. It can be used to estimate the quality of the predicted model parameters. It can be used to determine which model parameters, or which combinations of model parameters, are best determined. It can be used to determine which data are most important in constraining the estimated model parameters. It can determine the effects of noisy data on the stability of the solution. Furthermore, it can help in experimental design

by determining where, what kind, and how precise data must be to determine model parameters. Richardson (2003) describe the inversion theory as the (mathematical) process of predicting (or estimating) the numerical values (and associated statistics) of a set of model parameters of an assumed model based on a set of data or observations.

As it has been already described that relationship between data and model parameters are non-linear thus we don't have any algorithm to solve the non-linear inverse problem directly. So there is twofold target for solving non-linear inverse problem. First target is to reduce in a form which can be handled by the data fitting and model parameter estimation methods developed for linear problems. This procedure is called linearization. Second target is to find approximate meaningful solution of the problem and procedure is termed as model identification and appraisal. Gauss suggested that non-linear problems can be solved in successive approximations using the linear least-square method This involves the conversion the non-linear problem into an approximate linear form by expanding the function f(m) in Taylor series about an initial guess of the what the values the model parameters might be. This is the standard strategy adopted in geophysical inversion.

2.2.1 Linearization of Non-linear Problem

Most non-linear inversion schemes require as a starting point, the provision of some approximate values of the desired model parameters, which we shall simply call 'm_0'. This starting model may be based on a priori information or may be simply an intelligent guess. This initial model often results in difference between success and failure of finding a meaningful result or between slow and fast convergence to the solution.

Consider a general relationship between the data and the model parameters for non-linear problem is given by

$$d_i = g_i(m) \tag{2.9}$$

Next, assuming $g_i(m)$ is linear about m_0 such that a small perturbation of the model responses about m_0 can be expressed using Taylor's theorem as

$$d_i = g_i(m) = g_i(m_0) + \sum_{j=1}^{M}\left[\left.\frac{\partial g_i(m)}{\partial m_j}\right|_{m=m_0} \cdot \Delta m_j\right] + \sum_{j=1}^{M}\left[\left.\frac{\partial^2 g_i(m)}{\partial m_j^2}\right|_{m=m_0} \cdot \Delta m_j^2\right] + \cdots \tag{2.10}$$

where Δm is the difference between m and m_0,

$$\Delta m = m - m_0 \tag{2.11}$$

If it is assumed that terms in $\Delta m_j^n, n > 2$, are small with respect to δm_j terms and neglected higher order terms, an approximation which is valid only if series converges, then

$$d_i = g_i(m) = g_i(m_0) + \sum_{j=1}^{M}\left[\left.\frac{\partial g_i(m)}{\partial m_j}\right|_{m=m_0} \cdot \Delta m_j\right] \tag{2.12}$$

The predicted data $d_{i,obs}$ at $m = m_0$ are given by

$$d_{i,obs} = g_i(m_0) \tag{2.13}$$

$$d - d_{i,obs} = \sum_{j=1}^{M}\left[\left.\frac{\partial g_i(m)}{\partial m_j}\right|_{m=m_0} \cdot \Delta m_j\right] \tag{2.14}$$

Misfit = observed data predicted data

To estimate a meaningful 'm', we need to minimize this misfit as best as possible.

So we can write in the linear form of '$y = J \cdot x$'.

where;

$$x = \Delta m_j = m - m_0 \tag{2.15}$$

$$y = d_i - d_{i,obs} \tag{2.16}$$

Here, 'J' is called Jacobian or sensitivity matrix of partial derivative of 'g' with respect to each of model parameter 'm_j. The size of this matrix will be (m x n) for 'm' no. of data points and 'n' no. of model parameters. Now 'J' changes with each iteration. That is, one may obtain a different 'J' for each spot in solution space. Having to reform 'J at each step can be very computationally intensive, and often one uses the same 'J' for more than one iteration. Thus, by linearizing equation 2.9, we have arrived at a set of linear equations, where now the difference between observed and predicted data is a linear function of changes in the model parameters from some starting model. Now one can apply any algorithm which works for linear inverse problem.

2.2.2 Problem formation and regularization

Now there is need to reduce the difference between observed and predicted data as much as possible. As the least squares method gives mathematical robustness to the noisy data, it has been opted for minimizing the difference between observed and predicted data. This least square misfit function for non-linear inverse problem '$d = A(m)$' can be written as follows:

$$P(m) = (d - A(m))^T (d - A(m)) \tag{2.17}$$

Geophysical inversion problems are highly under-determined and ill-posed prob-

lem. Inversion operator in '$d = A(m)$' is non-linear and non-continuous for geophysical data. Due to dis-continuity of inverse operator, inverse problem is ill-posed. That means So we will wish to minimize the above misfit function. To make the problem well-posed, we need to regularize the above minimization function. Regularization of the problem stands for solving inverse problem for a regularized model parameter 'm_α' instead of true model parameter 'm' using a regularization parameter 'α' so that when 'α' tends to zero,'m_α' tends to 'm' and regularized inverse operator 'A_α' tends to true inverse operator 'A'. So now inverse problem will become like

$$m_\alpha = A_\alpha^{-1} d \tag{2.18}$$

Now misfit equation becomes:

$$P^\alpha(m) = (d - A(m))^T (d - A(m)) + \alpha(m - m_0)^T (m - m_0) \tag{2.19}$$

The regularization parameter a describes the trade-off between the best fitting and most reasonable stabilization. In a case where 'α' is selected to be too small, the minimization of the parametric functional 'P^α' is equivalent to the minimization of the misfit functional; therefore, we have no regularization, which can result in an unstable incorrect solution. When a is too large, the minimization of the parametric functional 'P^α' is equivalent to the minimization of the stabilizing functional, which will force the solution to be closer to the a priori model.

2.2.3 Gradient Algorithm

There are various algorithms to minimize this minimization problem. In this study we will focus on the steepest Descend, conjugate gradient, Gauss-Newton, Levenberg-Marquadt algorithm to solve the above minimization problem and we will compare the results we will get from above algorithms. Now we will discuss methodology,

14

advantages and limitations of above algorithms one by one.

Steepest Descend

The method of Steepest descent is a simple gradient method. In this method, the initial model is corrected in the direction of the negative gradient of the objective function 'P^α'.

$$x = -k \left(\frac{\partial P^\alpha(m)}{\partial m} \right) \tag{2.20}$$

Optimization problem for non-linear weighted least square method is

$$P^\alpha(m) = (d - A(m))^T (d - A(m)) + \alpha w^T w (m - m_0)^T (m - m_0) \tag{2.21}$$

To obtain the minimum of above equation, we take the derivative with respect to the model, set it to zero, and obtain the update:

$$\delta m = -k^\alpha I^\alpha(m) \tag{2.22}$$

$$I^\alpha(m) = J^T (A(m) - d) + \alpha w^T w (m - m_0) \tag{2.23}$$

$$k_n^\alpha = \frac{\|I^\alpha(m_n)\|^2}{\|J_{m_n} I^\alpha(m_n)\|^2 + \alpha \|w I^\alpha(m_n)\|^2} \tag{2.24}$$

$$m_{n+1} = m_n + \delta m_n = m_n - k_n^\alpha I^\alpha(m_n) \tag{2.25}$$

so $I^\alpha(m_n)$ describes the "direction" of increasing (ascent) of the functional $P^\alpha(m)$, in other words, the direction of "climbing on the hill." However, the new model m_{n+1}

may not fit our data adequately such that we may need to repeat the procedures using m_{n+1} as the new starting model. The successive application of this procedure is described as unconstrained iterative least square fitting. Where the Jacobian matrix 'J' is evaluated at m_{n+1}. It is obvious that replacing the constant factor k with $(J^T J)^{-1}$ will lead to the Gauss-Newton solution. The value of 'k' determine the step size of the corrections. Notice that above equation doesn't contain any inverse matrix. The scheme doesn't diverge and this is an advantage over the Gauss-Newton method. Provided 'k' is small enough. It has good initial convergence characteristics. A major drawback of this method of Steepest-descent is that the rate of convergence decreases as the least square solution is approached unlike the Gauss-Newton method. It is often inefficient requiring a large number of steps and is therefore less recommended for practical geophysical inversion applications.

Gauss-Newton

Gauss-Newton method is the successor of steepest gradient method. It also has same minimization function to be minimized as in above steepest descent method. The main idea of the Newton method is to try to solve the problem of minimization in one step:

$$m_1 = m_0 + \Delta m \tag{2.26}$$

Thus, instead of moving downhill along a long path formed by mutually orthogonal directions of the steepest descent, one can try to reach the minimum of the misfit functional along one direction.Taking the first variation of the parametric functional 2.21 with respect to model parameters and equating to zero, it will give gauss-newton update for the model parameters:

$$(J^T J + \alpha w^T w)\Delta m = -J^T(A(m) - d) + \alpha w^T w(m - m_0) \qquad (2.27)$$

Gauss-Newton algorithm converges much more rapidly than the steepest descent method. The main difficulty is that it is a rather complicated problem to calculate the inverse quasi-Hessian operator.

Conjugate Gradient

The conjugate gradient method is based on the same ideas as the steepest descent and the iteration process is very similar to the Gauss-Newton method. However, the "directions" of ascent are selected in a different way. On the first step we use the "direction" of the steepest ascent. On the next step the "direction" of ascent is a linear combination of the steepest ascent on this step and the "direction" of ascent on the previous step. For this case also we are solving same optimization equation 2.21.

Taking the first variation of the parametric functional with respect to model parameters and equating to zero, it will give gauss-newton update for the model parameters:

$$m_{n+1} = m_n + \delta m_n = m_n - k_n^\alpha \hat{I}^\alpha(m_n) \qquad (2.28)$$

$$I^\alpha(m) = J^T(A(m) - d) + \alpha w^T w(m - m_0) \qquad (2.29)$$

$$k_n^\alpha = \frac{\hat{I}_n^\alpha \cdot I_n^\alpha}{\|J_{m_n} I^\alpha(m_n)\|^2 + \alpha\|w I^\alpha(m_n)\|^2} \qquad (2.30)$$

$$\hat{I}_n^\alpha = I_n^\alpha + \beta_n^\alpha \hat{I}_{n-1}^\alpha \qquad (2.31)$$

17

$$\beta_n^\alpha = \frac{\|I_n^\alpha\|^2}{\|\hat{I}_{n-1}^\alpha\|^2} \qquad (2.32)$$

In general, nonlinear cases the number of iterations is not fixed, but still the method converges very Rapidly. Another advantage of the conjugate gradient method is that we go downhill not along a line, but on various planes. In this case we can overcome small local minima of the misfit functional and go faster directly to its global minimum.

Levenberg-Marquadt

The underlying philosophy here is that the parameter change may over-shoot the linear range (for a non-linear problem) if their absolute values are left unchecked. A bound is therefore placed on the size of the perturbations thereby constraining the Step-length of the solution. Here optimization function will be different than above methods:

$$P^\alpha(m) = (d - A(m))^T(d - A(m)) + \alpha(w(m - m_0)^T w(m - m_0) - L_0^2) \qquad (2.33)$$

Here, α is referred as damping factor.

Differentiating the above objective function with respect to model parameters and equating that to zero, we will get

$$(J^T J + \alpha I)\Delta m = J^T(d - A(m)) \qquad (2.34)$$

The solution is then used in an iterative process to fit our data. If our starting model is m0, non-linearity is dealt with using the iterative formula.

$$m_{n+1} = m_n + (J^T J + \alpha I)^{-1} \cdot J^T(d - A(m)) \tag{2.35}$$

This method is in effect a hybrid technique in the sense that it combines the steepest descent and Gauss-Newton method. Steepest descent method dominates when starting model is far from initial model whereas Gauss-Newton method dominates when solution is approached. The above algorithm has the disadvantage that if the value of l is large, the calculated Hessian matrix is not used at all. It is to be noted that while the LM method is in no way optimal but is just a heuristic, it works extremely well in practice. The only flaw is its need for matrix inversion as part of the update.

2.2.4   Compressed sensing algorithm

CS theory asserts that one can recover certain signals and images from far fewer samples or measurements than traditional methods use. To make this possible, CS relies on two principles: sparsity, which pertains to the signals of interest, and incoherence, which pertains to the sensing modality. CS exploits the fact that many natural signals are sparse or compressible in the sense that they have concise representations when expressed in the proper basis. Incoherence says that unlike the signal of interest, the sampling/sensing waveforms have an extremely dense representation in . In this study CS theory has been used to use the signal recovery algorithms of CS theory to reconstruct the conductivity distribution. The prior condition of signal recovery required by CS theory is that the original signal can be sparsely represented. Studies have shown that normal L2 -regularized method always imposes smoothness in order to obtain stability in the reconstruction process, but it is not ideally suitable for reconstructing object with a sharp transition in conductivity distribution. For L1 regularization, the sparsity of the solution reduces the redundancy informa-

tion, which leads to obtain better edge sharpness and fewer image artifacts. Thus the imaging algorithm here is based on 1 L regularization, which may improve its imaging accuracy.

It states that if a signal is sparse or approximately sparse in some orthonormal basis, then it can be accurately reconstructed from the fewer number of randomly sampling signal, which breaks through the Shanon-Nyquist sampling theory in some sense. Given an unknown signal vector f of size (n x 1), an observer can be obtained through m measurements, where each measurement is the inner product between the signal f and a known sensing matrix A of size (m x n). Thus the mathematical model is

$$y = \langle f, v \rangle + v \tag{2.36}$$

where, 'v' represents the observation noise, $\langle f, v \rangle$ is the inner product of matrix 'A' and vector 'f'. The prior condition of CS is the signal 'f' is sparse or can be sparsely represented. When 'f' is a sparse signal, 'A' can be a randomly sampling matrix ϕ. The vector 'f' can be recovered from the measurements using the convex optimization function as follows:

$$\min \|y - Af\|_2^2 + \lambda \|f\|_1 \tag{2.37}$$

where, λ is a regularization parameter. When 'f' is not a sparse signal, it should be sparsely represented as

$$f = \varphi x \tag{2.38}$$

where 'x' is a sparse vector, and φ is often an orthogonal matrix. Thus the sensing matrix 'A' should be composed by a sampling matrix ϕ and an orthogonal matrix φ. The convex optimization has the form as

$$\min \|y - Ax\|_2^2 + \lambda\|x\|_1 \qquad (2.39)$$

where, $A = \varphi\phi$, and λ is the regularization parameter. The problem is reformulated as the recovery of a sparse signal x from y and A. Above equation is solved using the primal-dual interior point method. Then the signal 'f' can be obtained through transformation as 'f $= \varphi$ x'. In order to obtain sparse representation of the signal f, discrete cosine transform (DCT) is chosen as the orthogonal matrix φ.

In the previous section, all the algorithm uses L2 norm minimization which is not ideally suitable for the problem with a sharp transition in conductivity distribution, as it always imposes smoothness in order to obtain stability in the reconstruction process. However, studies have shown that L1 -regularized method can perform well with sharp transition conductivity. In L1 -regularized least squares program, the object function often combined with L2 and L1 norm to optimize the solution, which has the form as

$$\min \|\Delta d - J\Delta m\|_2^2 + \lambda\|\Delta m\|_1 \qquad (2.40)$$

where, second part denotes the L1-norm of the vector Δm and $\lambda > 0$ is the regularization parameter. Several algorithms have been proposed for solving L1 -regularized least squares program, such as coordinate wise descent methods, barrier method, gradient projection algorithms and so on. The same algorithm that used in signal recovery part is applied here for image reconstruction. In order to compare with the L1 -regularized algorithm, Regularized conjugate gradient algorithm, regularized steepest descent algorithm, Regularized Gauss-Newton algorithm, Levenberg-Marquadt algorithm are used during inversion process.

2.3   MATLAB Implementation

All codes has been developed in MATLAB within the framework of RESINVM3D package. All of the source code has been developed in MATLAB. This was done for two main reasons: MATLAB source code is platform independent, so any user can download the source code and run the driver files without the need to recompile. MATLAB has excellent built-in graphical support, allowing the user to easily produce a variety of different 3D renderings of the resulting models. Matlab codes has been developed for Steepest gradient, conjugate gradient, Levenberg-Marquadt, Compressed sensing algorithm. RESINVM3D had already developed code for inexact gauss-newton algorithm. Explicit calculation of sensitivity matrix is computationally very expansive and in this study, a methodology has been developed to explicitly calculation of sensitivity matrix. According to Haber(2000), to create sensitivity matrix, we need to differentiate the discretized equation 2.3; with respect to 'm' (assuming u = u(m) as in unconstrained formulation. This gives

$$\frac{\partial(A(m)u(m))}{\partial m} = G + A\frac{\partial u(m)}{\partial m} = 0 \tag{2.41}$$

Thus derivative of predicted data with respect to model parameters is

$$\frac{\partial d}{\partial m} = \frac{\partial(Qu)}{\partial m} = QA^{-1}B = J \tag{2.42}$$

Haber(2000) [21] states that for calculating $J \cdot v$; we don't need to calculate 'J' explicitly but in Compressed sensing application, we must need explicit calculation of sensitivity matrix 'J'. If above equation will be followed for calculation of sensitivity matrix 'J', then one has to solve linear inverse problem many times using bi-conjugate stabilization because for calculating 'B', we are calculating derivative of S(m) with respect to model parameters and calculating 'B' explicitly will again be complicated. So we have gone other way round for calculation of sensitivity matrix by calculating

22

transpose of sensitivity matrix instead of calculating sensitivity matrix.

$$J^T = (A^{-1})^T \cdot Q^T \cdot G^T \tag{2.43}$$

The effect of this technique is now we have to solve linear equation one time for

$$s = (A^{-1})^T \cdot Q^T \tag{2.44}$$

Now one can just multiply this calculated 's' with the 'G^T' to get transpose of sensitivity matrix. After the calculation of transpose of sensitivity matrix, we can easily calculate the sensitivity matrix too. So this will save time and computational cost in calculation of sensitivity matrix. Now for the application of Compressed sensing algorithm, we have used open source matlab code 'l1-ls.m' which uses primal-dual interior point method for solving optimization problem. This method solves l2 norm minimization with l1-norm regularization. We have used Discrete Cosine Transformation as orthogonal matrix to make the signal or for our case 'change in model parameter' sparse. We have used in-built function 'dctmtx' for obtaining orthogonal matrix.

2.4   Synthetic Problem

We have tested and analyzed our code on various synthetic models. We have used 40 electrodes having 8 and 5 electrodes in x and y directions respectively. We have kept x and y spacing as 0.4 m and 0.7 m respectively between electrodes so that we can form a grid of size 2.8 x 2.8 m square grid. We have created 134 combination of current and potential electrodes using dipole-dipole to measure 134 data point over whole volume. We discretized the volume using finite volume method. We have created 134 data points using forward modeling algorithm used in RESINVM3D (citation). In

the result section, we will see the different discretization used in various cases. We have used different synthetic problem for different scenarios. We have varied resistivity values in the vertical direction, spatial direction to test the behavior of various algorithms under these conditions. We have also tested the behavior of algorithm under different level of under-determinacy i.e. increasing the model parameters and keeping the number of data point same. By increasing model parameter, we wanted to induce more sparsity in the nature of the model. We have compared other two synthetic cases where one model has more sparsity in structure and other has less. Last two cases we have tested to see the effect of sparsity on the inversion of the model using compressed sensing.

Chapter 3

Modelling Soil-Water-Disease Interaction of Orange Tree

3.1 Problem Description

Orange trees develop in response to genetic endowment, climate, and cultural practices including irrigation and nutrition. Low crop yield in the Vidarbha region is attributed to erratic climate conditions and improper management activities, resulting in the formation of water mold disease called 'root rot' or 'Gummosis' (Phytophthora spp.). Under favorable conditions (high soil moisture and cool temperature), the disease causing bacteria produces large numbers of motile zoospores that can swim and transports in water to the roots. These zoospores contact the root system they encyst, germinate and enter the root tip resulting in rot of the entire rootlet. Gummosis occurs when these zoospores splash onto a wound or bark crack around the base of the trunk. It is almost impossible to identify the early stage symptoms of this disease, and hence, making it difficult to implement effective management actions. Late stage impressions of a gummosis effected tree are seen at the surface, with symptoms in-

cluding leaf-less branches, yellow foliage, shoot die-back, reduced fruit size and yield, thin canopy, failure to make new growth, little water and nutrient uptake leading to wilting.

In this study, we have tried to differentiate the characteristics of diseased and healthy tree based on root water uptake capacity under the same hydro-geological scenario. For this purpose, we have simulated water flow using axi-symmetric form of Richard's equation which has sink term in its equation. Total root water uptake is used as sink term in the water flow model. This analysis has been done for water flow in the root zone of both healthy and diseased tree.

3.2 Experimental Setup

ERT is proven to be an effective method for measuring soil-moisture distribution within the root zone of citrus trees (Binley and Kemna, 2005,[22]). A square grid of 2.8 m x 2.8 m with orange tree located at the center was laid with 40 surface electrodes placed at the nodes of the grid. Spacing of nodes in x- and y- directions respectively are 0.4 m and 0.7 m, thus making a grid of 5 (rows) x 8 (columns). The geometry of electrodes was considered in such a way that resistivity characterization is possible for the entire plot with highest sounding sensitivity achieved in the top one meter of soil. Surface electrodes were penetrated to a depth of 10 cm to reduce noise in the data. Two multi-electrode cables were used to connect the electrodes of the grid with ABEM Terrameter Lund system to perform ERT experiment. We developed a 3-D protocol system with dipole-dipole configuration to suit the grid architecture and has been validated using series of 2-D measurements, before taking actual measurements. Each tree is provided with 4-time domain reflectometer (TDR) soil moisture probes located at 40 cm from the grid edge and placed at 4 different depths (15, 30, 45, and 60 cm below ground level). ERT derived soil moisture data is in close agreement
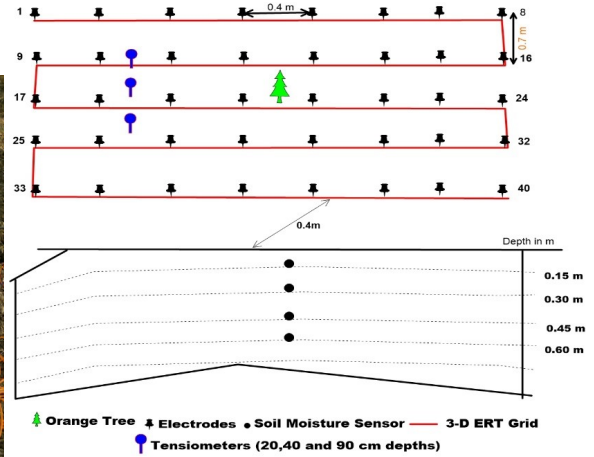
(a) actual field setup   (b) Diagram of field set up

with TDR measurements and hence, considered as observed soil moisture data for use with numerical calibration. Three tensiometers were installed beneath the two experimental plots (at depths 20 cm, 40 cm, and 90 cm with horizontal spacing of 20 cm) to monitor hydraulic heads. Tensiometer depths were considered to ensure that hydraulic gradient within and beyond the root zone were completely captured. Water fluxes crossing the bottom boundary of each experimental plot were estimated using Darcy's law [23].

3.3 ERT Monitoring of Soil Moisture Fluxes

Classical methods of estimating soil moisture content in the near surface zone, such as gravimetric (Sharp and Davies, 1985) , neutron probes, and time domain reflectometry (TDR) [24] are expensive, provides point estimate, and are destructive in nature. In contrast, remote sensing techniques though provide soil moisture distribution over larger areas without soil destruction, suffer from the drawbacks of low resolution and depth of penetration. Knowing the fact that soil electrical conductivity is the best proxy for moisture content and solute concentration ([25] [26]), electrical resistivity tomography (ERT): a non-invasive, proximal, geo-physical technique has been widely

used in the recent past for characterizing soil-water dynamics in the rhizosphere. Many studies have shown that ERT can be suitably applied to monitor soil moisture and root water uptake (RWU) distribution at local to field scale ([27] , [26], [28], [29], [22]). However, ERT derived soil moisture data has to be validated at the point locations (gravimetric or TDR probes) that are spatially distributed within the root zone before numerically characterizing root water distribution in spatio-temporal domain ([30], [31],[28], [22]).

To develop the non-linear relation between resistivity and soil moisture applicable for the given soil, we estimated modified Archie's law parameters using laboratory studies following ASTM guidelines (ASTM G 57-95,1995). Archie's law can be written in mathematical form in following equation:

$$\rho = a \cdot \rho_w \cdot \theta^{-m} \tag{3.1}$$

where

ρ= resistivity;

θ = soil moisture content;

ρ_w = resistivity of fluid used in measurement;

a,m = parametric constant depending on soil properties;

We can write this equation as

$$\rho = A \cdot \theta^{-m} \tag{3.2}$$

where;

A,m = Empirical constant depending on soil type

But Archie's law has been developed for coarse grained soil or sandy soil. But in our study, soil has significant amount of clay content, so we have used modified form of Archie's law which has been given by Waxman & Smits model. Waxman & smits

model can be written in mathematical form as

$$\sigma = a \cdot \theta^c + b \qquad (3.3)$$

where,

a,b,c=emperical constant depending on soil type

σ =conductivity of the soil

For obtaining empirical constants, a, b, c; we have collected soil samples at four depths (4-17 cm, 17-30 cm, 30-43 cm, 47-60 cm) and calibrated Waxman & Smiths model for four samples separately. Four acrylic cylindrical mould (of 120 mm length and 80 mm diameter), each for one depth, with porous plates at the ends was filled with homogeneous soil, compacted in layers to achieve the undisturbed structure of the soil. Four mini stainless steel electrodes penetrating for a depth of 10 mm (2 current electrodes on either side of the mould, and 2 potential electrodes along the length) were used to measure soil resistivity changes in response to moisture variations. Potential electrodes are kept at a spacing of 40 mm. The laboratory set up for estimating Waxman & Smiths model parameters (a, b, c) is given in Figure 2. ABEM Terrameter Lund system was used to measure resistivity for a given soil moisture condition. We started the measurement of resistivity at a fully saturated condition and observed resistivity at each stage of moisture content from saturation to residual moisture content. The decrease in the soil moisture for each observation period is ensured by allowing the soil to naturally dry and keeping it airtight for next 12 hours to achieve homogeneous moisture content all over the volume.

3.4 Development of soil-water retention curve

Unsaturated soil hydraulic parameters were obtained by developing water retention curves for soil horizon at 30cm depth. Modified version of Archie's law [32], Waxman

(a) actual laboratory setup
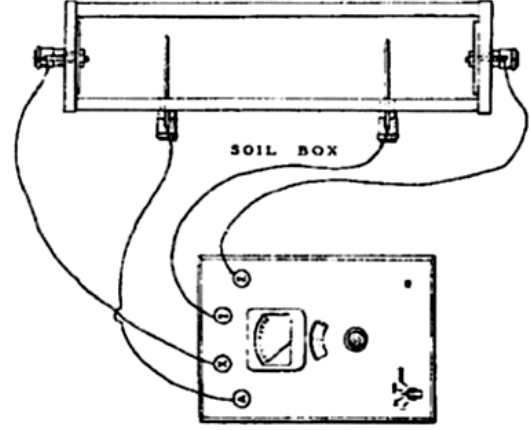
(b) ASTM standard laboratory set up

and Smits [33] model was fitted to the data, and the model parameters were estimated using multi-step outflow experiments following Retzlaff, et al. (1985) . A plastic cylinder of 5-liter capacity with drainage holes at the bottom was used to plot soil-water retention curves. A field soil of about 4 kg was filled in the cylinder for about 20 cm depth with tensiometer placed at the center. Tensiometer was filled with blue liquid to avoid algae growth during the laboratory examination. The experiment was carried out between saturated water content ($_s$) and residual water content ($_r$) in stages by naturally drying the soil, and lapsed for about 9 days. Initially, the soil is fully saturated by restricting gravitational flow through the drain holes, and the initial hydraulic equilibrium condition between tensiometer cup and the surrounding soil, was precisely established. During each stage, both volumetric water content and soil suction were recorded. Water content in each stage is estimated using gravimetric method [34]. Van Genuchten model parameters 'α' and 'n' were estimated by fitting soil water retention model to the observed drainage curve data using RETC code that considers the constitutive relationships given by

$$\theta(\psi) = \begin{cases} \theta_r + \frac{\theta_s - \theta_r}{[1+(|\alpha_v \psi|^n)]^m}, & \text{if } \psi < 0 \\ \theta_s, & \text{if } \psi \geq 0 \end{cases}$$

30

$$K(\psi) = K_s S_e^l \left[1 - (1 - S_e^{(1/m)})^m \right]^2 \tag{3.4}$$

Where;

θ_r & θ_s= residual and saturated soil water contents respectively ($cm^3 cm^{-3}$);

α_v = reciprocal of the air entry;

$m = 1 - \frac{1}{n}; n > 1$

n = pore-size distribution index;

S_e = effective saturation;

l = pore-connectivity parameter;

K_s = saturated hydraulic conductivity ($cm day^{-1}$)

3.5 Modelling Root Water Uptake using HYDRUS

Axi-symmetric form of Richards equation describing variable saturated flow was used to simulate root water uptake (RWU) from the orange trees. We used HYDRUS (2D/3D) to simulate transient movement of water flow and RWU processes in an isotropic, heterogeneous, variably saturated flow domain. Details on HYDRUS (2D/3D) simulation is can be found in the HYDRUS theoretical document ([35], [36]). Neglecting the effect of air phase on water flow, the governing equation for flow is given by:

$$\frac{\partial \theta}{\partial t} = \frac{1}{r}\frac{\partial}{\partial r}\left(rK\frac{\partial \psi}{\partial r} \right) + \frac{\partial}{\partial z}\left(K\frac{\partial \psi}{\partial z} \right) - \frac{\partial K}{\partial z} - S(\psi, r, z) \tag{3.5}$$

where

t is simulation time (d);

r is radial distance from the trunk (cm);

z is simulation step in vertical direction (positive upward) (cm);

ψ is pressure head (cm);

K is unsaturated hydraulic conductivity function (cmd^{-1});

S(,r,z) is RWU from the model, represented as sink term and given by

$$S(\psi, r, z) = \alpha(\psi, r, z) \times S_p(r, z) = \alpha(\psi, r, z) \times b(r, z) \times T_p \times L \qquad (3.6)$$

where $\alpha(, r, z)$ is the water stress response function (dimensionless), the factor by which actual RWU reduces, and can be estimated using piece-wise linear reduction function proposed by Feddes [37].

$S_p(r, z)$ is the potential RWU;

b(r,z) is normalized water uptake distribution (cm^{-2})

T_p is potential transpiration rate (cmd^{-1})

L is the surface length associated with transpiration.

We adopted the 2-D axi-symmetric root water uptake model proposed by Vrugt [38] in estimating the normalized water uptake distribution given by,

$$S(r, z) = \left[1 - \frac{z}{z_m}\right]\left[1 - \frac{r}{r_m}\right] \exp^{-(\frac{P_z}{z_m}|z^*-z| + \frac{P_r}{r_m}|r^*-r|)} \qquad (3.7)$$

where

r_m and z_m are the maximum width and depth of the root zone (L) respectively,

z^* and r^* are the location of the maximum root water uptake, from the soil surface in the vertical direction

(z^*) and from the tree position in the horizontal direction (r^*),

p_r and p_z are the empirical coefficients.

Normalizing the uptake distribution ensures that b(r,z) integrates to unity over the flow domain. We optimized the root distribution parameters for both healthy and decline orange trees according to above equation to match the observed soil water content from ERT and simulated soil water content from HYDRUS. The reduction of

root water uptake due to the water stress $\alpha(h)$ was described using the well-known piecewise linear relation, developed by Feddes[37]:

$$\alpha(h) = \begin{cases} 0, & \text{if } h > h_1 \text{or} h \le h_4 \\ \frac{h-h_1}{h_2-h_1}, & \text{if } h_2 < h \le h_1 \\ 1, & \text{if } h_3 < h \le h_2 \\ \frac{h-h_4}{h_4-h_4}, & \text{if } h_4 < h \le h_3 \end{cases}$$

Where h_1, h_2, h_3, h_4 are the threshold parameters. Water uptake is at the potential rate when the pressure head is between h_2 and h_3, decreases linearly when $h > h_2$ or $h < h_3$, and becomes zero when $h < h4$ or $h > h1$. The following parameters of the Feddes et al. (1978)[37] model were used: ($h_1 = -10, h_2 = -25, h_{3,max} = -200, h_{3,min} = -1000, \& h_4 = -8000 cm$) and it was taken from [39] for Orange Tree.

For $\alpha(, r, z)$, the functional form of RWU parameters given by Feddes [37] with no water stress compensation was used in the simulation. Since, HYDRUS demands the daily evaporation (E_p) and transpiration (T_p) to be input separately along the atmospheric boundary, we have estimated daily reference evapo-transpiration (ET_0) using FAO-56 based Penman-Monteith equation [1] and partitioned into (E_p) and (T_p) using the FAO-56 based dual crop coefficient method [1]. Daily meteorological data was collected from an automatic weather station installed located at about 100 m from the experimental site. Actual crop evapo-transpiration (ET_c) for the citrus crops is estimated as:

$$ET_c = (K_{cb} + K_e) \times ET_0 \tag{3.8}$$

Where K_{cb} is the basal crop coefficient, taken from FAO-56 assuming 70% canopy and no ground cover in citrus orchard, and K_e is the evaporation coefficient. Potential evaporation and transpiration used in HYDRUS simulation are given respectively as:

$$T_p = (K_{cb}) \times ET_0 \tag{3.9}$$

$$E_p = (K_e) \times ET_0 \tag{3.10}$$

Chapter 4

Results and Discussions

4.1 Inversion of 3D resistivity Model

MATLAB code has been developed for Steepest gradient, Conjugate Gradient, Levenberg-Marquardt algorithm for the inversion in the framework of open source MATLAB package RESINVM3D. In RESINVM3D package, inexact Gauss newton algorithm has been implemented for the inversion. All of the above algorithms are tested and verified using various type of synthetic problems.

Case 1: Comparison of Gradient Algorithms and Compressed Sensing algorithm for ERT inversion:

In this case, synthetic model has been created using 561 cells ($17 \times 11 \times 3$) i.e. 17 cells in x-direction, 11 cells in y direction with 3 levels in z-direction. It is further discretized into cell size of 0.2 m in x-direction, 0.35 m in y-direction, and varied thickness of layers (0.25, 0.30, 0.40) in z-direction. Steepest gradient, Conjugate

Gradient, gauss newton, Levenberg-Marquardt, Compressed sensing algorithm are compared to test the convergence quality of each algorithm and the normalized root mean square error (range: -inf to 1) between synthetic model and inverted model has been observed. In this case, we have observed that Levenberg-Marquardt (0.418) giving marginally better value compared to other algorithm which are Gauss-newton (0.3972), Compressed sensing (0.3362), Steepest- descent (0.255) and Conjugate gradient (0.2378). So we can say that in this case gradient based algorithm performed slightly better than Compressed sensing algorithm. (figure- 4.1).

Case 2: Comparison of Algorithms when heterogeneity exists in depth:

In this case, synthetic model has been created using finer discretization with 4805 cells ($31 \times 31 \times 5$) i.e. 31 cells in x-direction, 31 cells in y direction with 5 levels in z-direction. Discretization has been done so that cell sizes are 0.2 m in x-direction and 0.35 m in y-direction, whereas in z-direction, thickness of layers (0.1, 0.2, 0.3, 0.4, 0.5) are varied top to bottom. In doing so, the difference between number of data points and model parameters has been increased to see the effect of under-determinacy on the convergence using various algorithms. Heterogeneity has been induced in depth as we provided different resistivity value for each layer. The resistivity values for first, second, third, fourth, fifth layer from top are 10 ohm-m, 50 ohm-m, 100 ohm-m, 200 ohm-m, 200 ohm-m respectively. Again in this case also, gauss newton, Levenberg-Marquardt, Compressed sensing algorithm has been compared to test the convergence quality of each algorithm and the normalized root mean square error (range: -inf to 1) between synthetic model and inverted model were observed. In this case, it is observed that compressed sensing algorithm (NRMSE = 0.7859) has outperformed other gradient based algorithm like gauss-newton (NRMSE = 0.467) and Levenberg-Marquadt (NRMSE = 0.0785). So it can be said that when model parameters (4805) are very high in comparison to data points (134) then compressed sensing algorithm performed
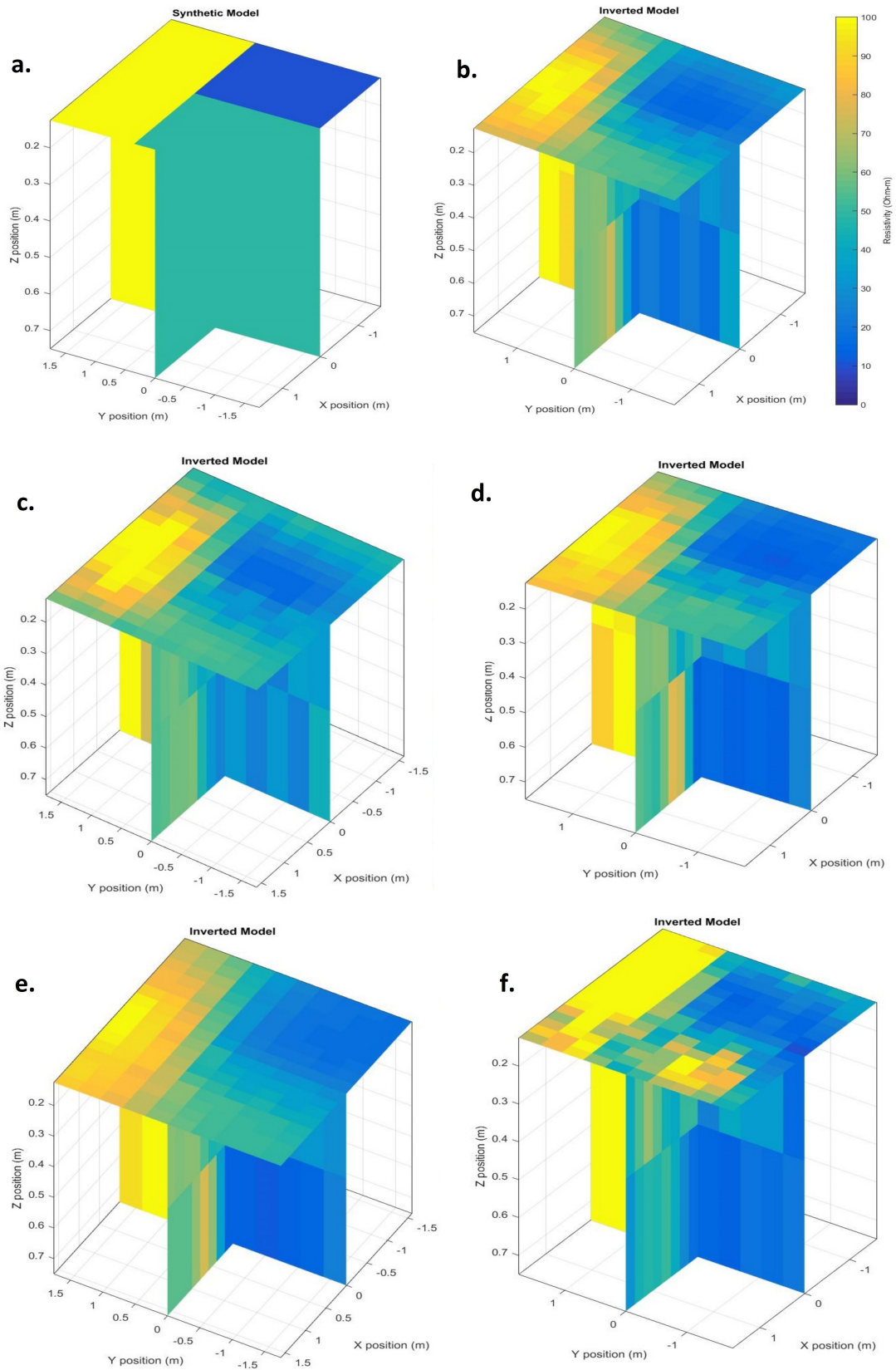
Figure 4.1: Comparison of algorithms: (a.) Synthetic model, and Inverted models using (b.) steepest gradient (c.) conjugate gradient, (d.) Levenberg-Marquardt, (e.) Gauss-Newton, (f.) Compressed sensing

better than conventional gradient based algorithms. (figure-4.2). Compressed sensing algorithm have detected all the layers effectively where Gauss-Newton and Levenberg-Marquardt algorithm failed to detect resistivity of first layer effectively.

Case 3: Comparison of Algorithms when heterogeneity exists in spatial direction:

In this case also, same discretization as case-2 has been kept but has been provided different resistivity zones in the same layer and kept same resistivity pattern throughout the depth so that variation in resistivity exist in spatial direction only. A vertical strip of high resistivity zone of 200 ohm-m has been sandwiched between two vertical strips of low resistivity zone of 25 ohm-m (figure 3a). Again in this case also, gauss newton, Levenberg-Marquardt, Compressed sensing algorithm has been compared to test the convergence quality of each algorithm and the normalized root mean square error (range: -inf to 1) between synthetic model and inverted model were observed. In this case, it is observed that compressed sensing algorithm (NRMSE = 0.5737) has outperformed other gradient based algorithm like gauss-newton (NRMSE = -0.2698) and Levenberg-Marquadt (NRMSE = -0.3317). Even after a large iteration and different regularization parameter values, gradient based methods were unable to detect the model properly. This case gave strength to the hypothesis that compressed sensing algorithm works well in comparison to other gradient based algorithms when model parameters (4805) are very high in comparison to no. of data points(134). (figure-4.3).

Case 4: Effect of Model Refinement on ERT inversion using Compressed sensing:

In this case, two synthetic models has been with different discretization of model. In the first case, 561 model cells ($17 \times 11 \times 3$) were used whereas in second case it had 4085
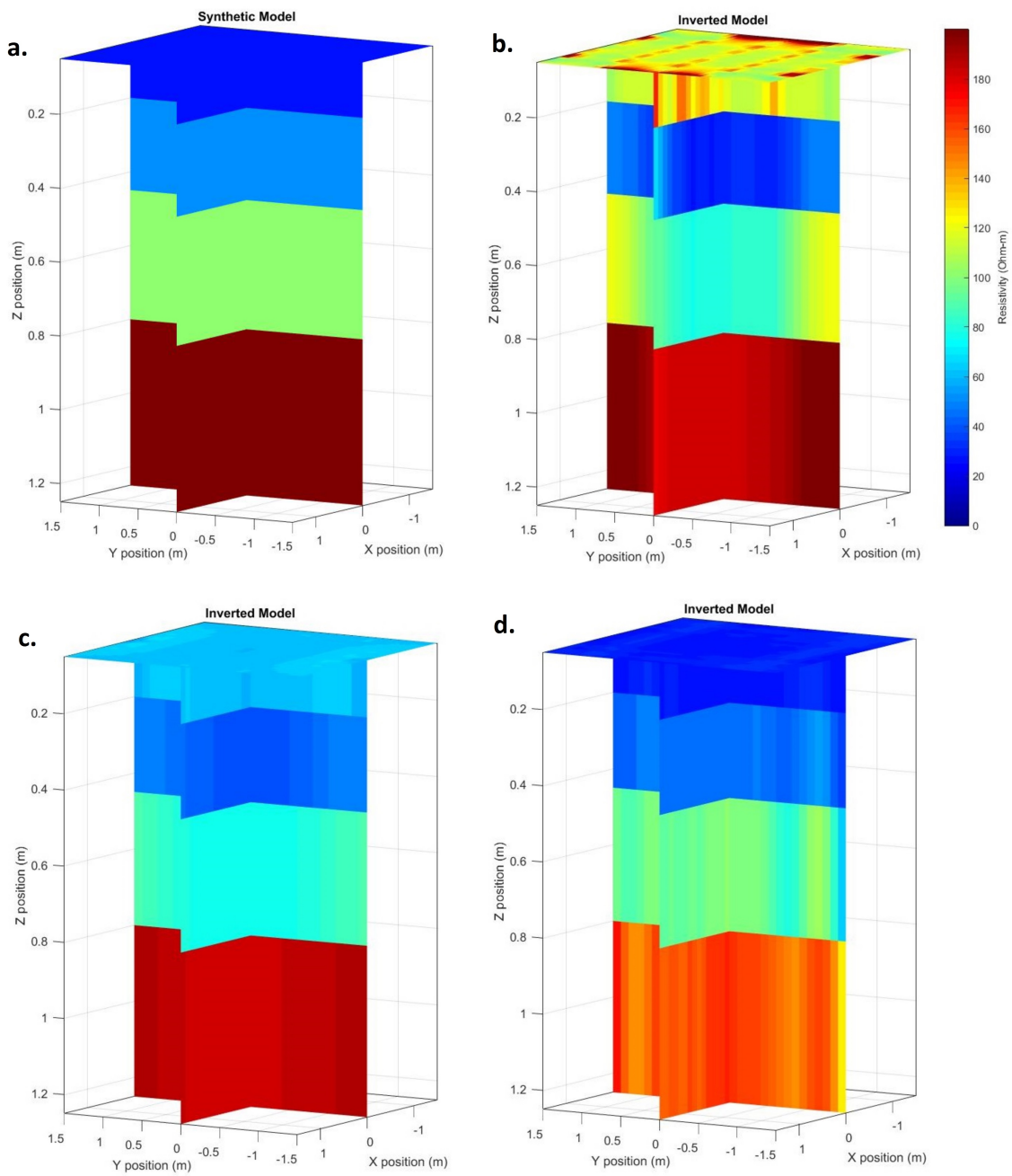
Figure 4.2: Comparison of Algorithms when heterogeneity exists in depth. (a.) Synthetic model, and Inverted models using (b.) Levenberg-Marquardt, (c.) Gauss-Newton, (d.) Compressed sensing
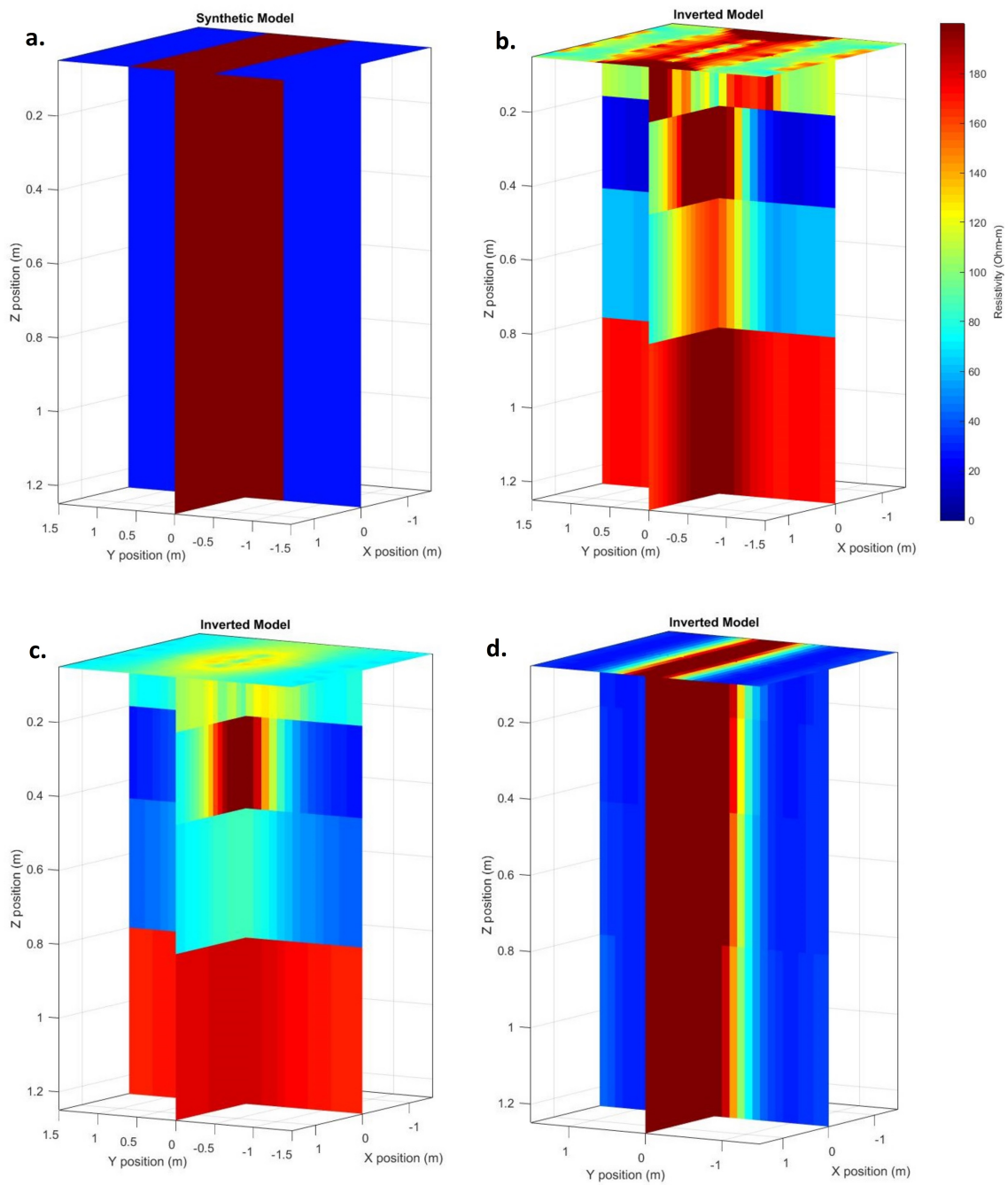
Figure 4.3: Comparison of Algorithms when heterogeneity exists in spatial direction. (a.) Synthetic model, and Inverted models using (b.) Gauss-Newton, (c.) Levenberg-Marquardt, (d.) Compressed sensing

model cells ($31 \times 31 \times 5$). In the first case, cell size were 0.2×0.35 m in lateral direction and varied depth of 0.25, 0.30, 0.40 in vertical directions whereas in second case cell sizes were 0.1×0.1 m in horizontal direction whereas depths of cell varied as 0.1, 0.2, 0.3, 0.4, 0.5 for first, second, third, fourth, fifth layer from top. In this case a very low resistivity zone of 25 ohm-m in the middle third portion has been surrounded by high resistivity zone of 200 ohm-m. it is observed that normalized root square error between synthetic model and inverted model is better in second case (NRMSE = 0.3843) where discretization is finer than the first case (NRMSE = 0.2883). Result of synthetic problem in this case gives an indication that compressed sensing algorithms converges the solution better when model discretization are finer.(fig 4.4)

Case 5: Effect of Model sparsity on ERT inversion using Compressed sensing:

In this case, two synthetic model having same discretization has been used but level of sparsity at some orthonormal basis are different. For first synthetic model, zones of different resistivity value (10, 25, 50, 100 and 200 ohm-m) were kept arbitrarily in the model to make the model less sparse. In the other synthetic model, two low resistivity zones of 10 ohm-m were kept in a region of high resistivity zone of 200 ohm-m. It is observed that in second case (NRMSE = 0.3753) normalized root mean square error is better than first case (0.2642). So when model is less heterogeneous then compressed sensing algorithm converged more effectively. (fig-4.5)
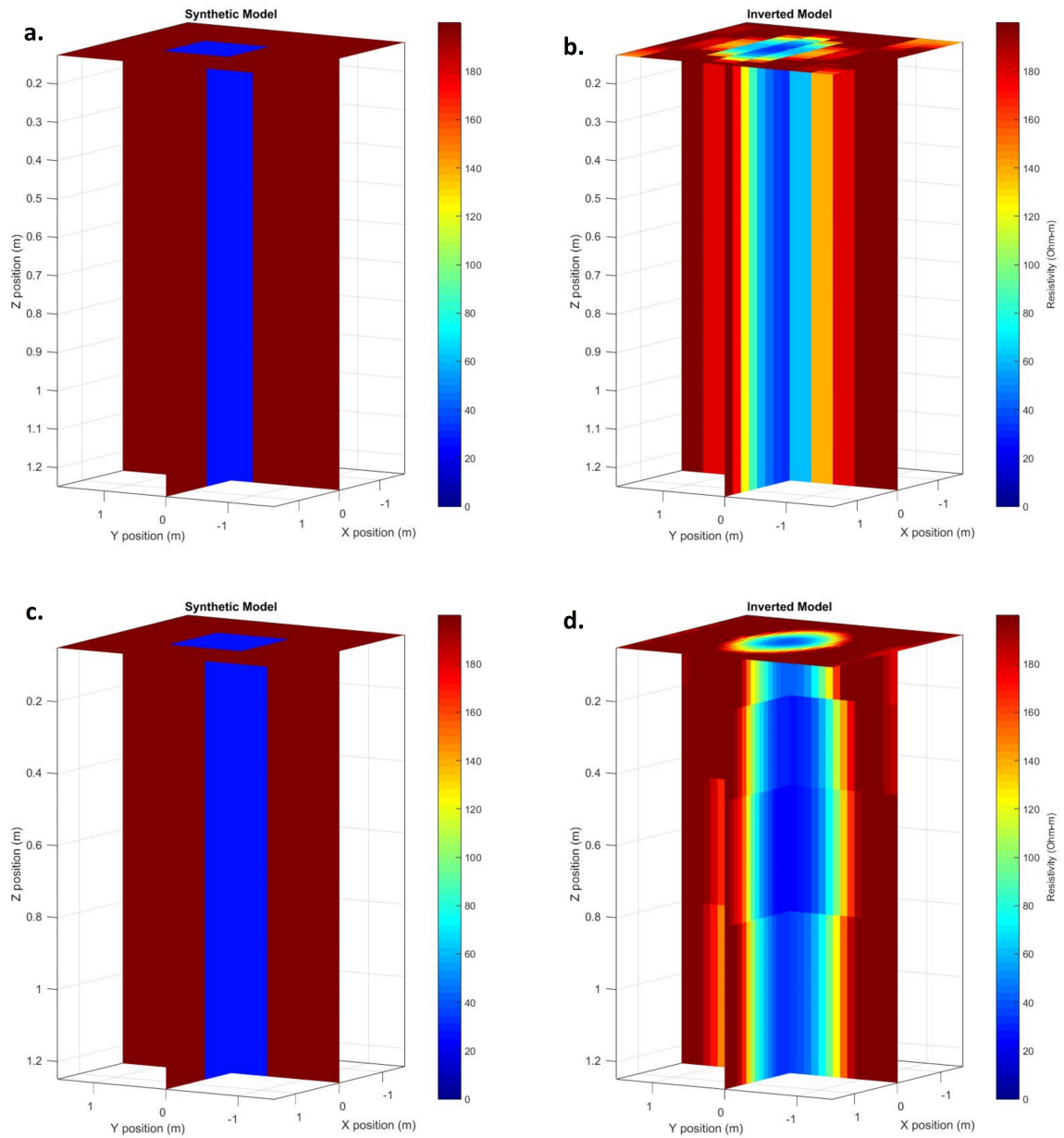
Figure 4.4: Effect of Model Refinement on ERT inversion using Compressed sensing. (a.) Synthetic and (b.) Inverted model when no.of parameters are 561 and (c.) Synthetic and (d.)Inverted model when no. of parameters are 4805.
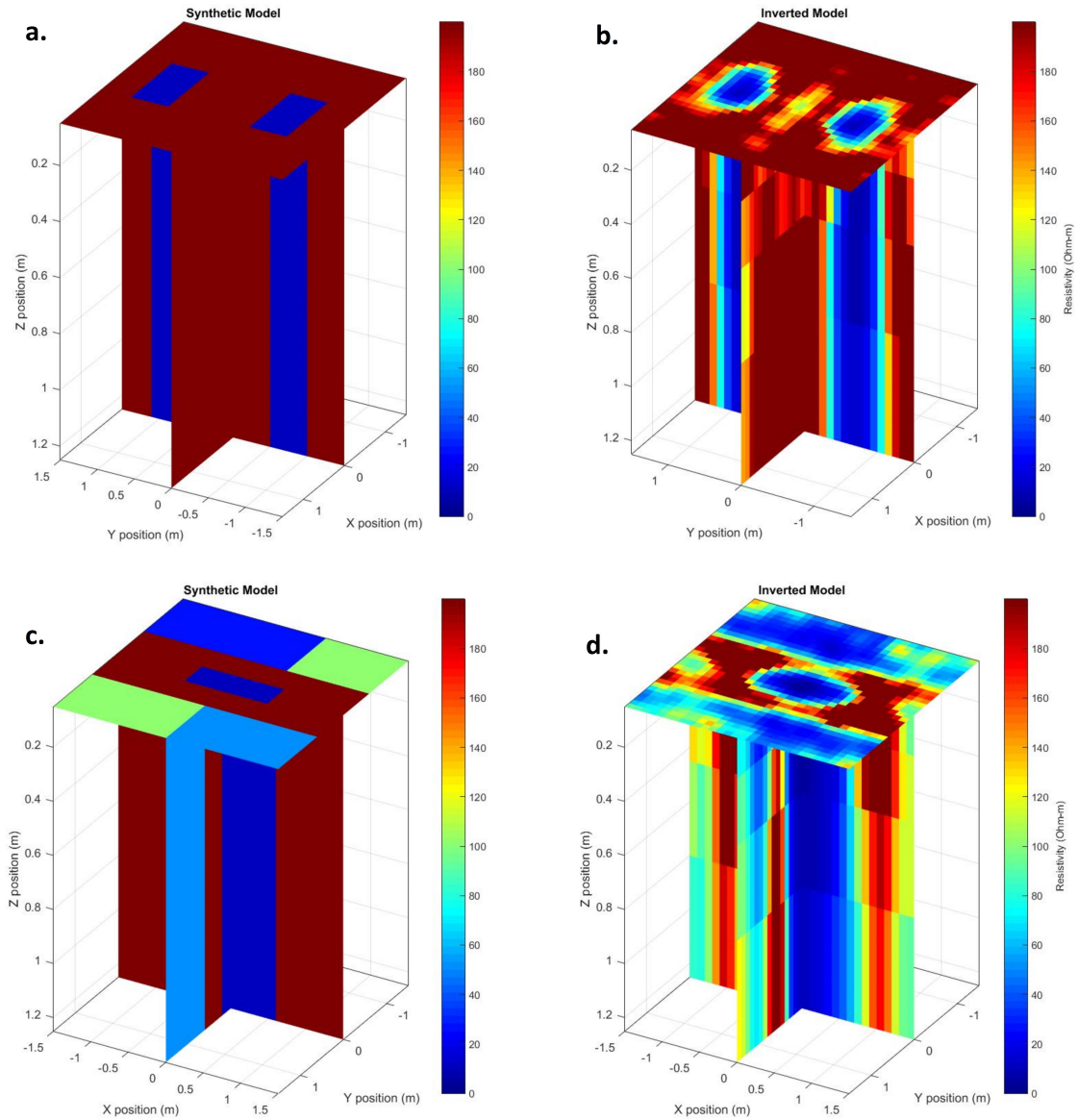
Figure 4.5: Effect of Model sparsity on ERT inversion using Compressed sensing. (a.) Synthetic and (b.) Inverted model when it has less heterogeneity and (c.) Synthetic and (d.)Inverted model when it is more heterogeneous.

4.2 Modelling Soil-Water-disease Interaction

4.2.1 Soil moisture - Resistivity Relationship

First physical properties of the soil has been obtained to reconstruct the soil structure as undisturbed. Density bottle method has been used for measuring specific gravity of the soil. Rest of the properties are obtained using gravimetric analysis. As four samples had been collected at four different depths, different physical properties has been obtained for each depth. properties are given in table 4.1. After obtaining physical properties, soil is placed into the acrylic mould and measured resistivity values at each level of water content as discussed in methodology part. Relation between resistivity and moisture content has been plotted using Waxman-smits model [33]. All graphs show very good relationship between moisture content and resistivity of sample. Significantly different relationship has been observed for soil sample at 30-43 cm depth which may represent the maximum root activity zone. Coefficients 'a', 'b' and 'c' are given in table 4.2. Graphical representation of relationship between resistivity and moisture content for soil sample at each depth has been given in figure 4.6. Above equations allows us to direct translation of 3-D resistivity distribution to a corresponding distribution of volumetric water content. For greater depth of 60 cm same equation (at 47-60 cm depth) was used up to 1 m to convert soil water content from resistivity data.

Table 4.1: Physical Properties of soil.

Parameter	Sample 1 (4-17 cm)	Sample 2 (17-30 cm)	Sample 3 (30-43 cm)	Sample 1 (47-60 cm)
Dry density (g/cc)	1.207	1.283	1.318	1.36
Bulk density(g/cc)	1.643	1.745	1.767	1.824
Moisture content(%)	43.55	46.235	44.8	46.6
Porosity	0.544	0.55	0.538	0.529
Sp. gravity	2.511	2.58	2.6165	2.56

Time-lapse ERT profiles were carried out at frequent intervals and for every case we have maintain before and after irrigation scenarios for both healthy and decline

Table 4.2: Waxman-Smit's model parameter values and RMSE

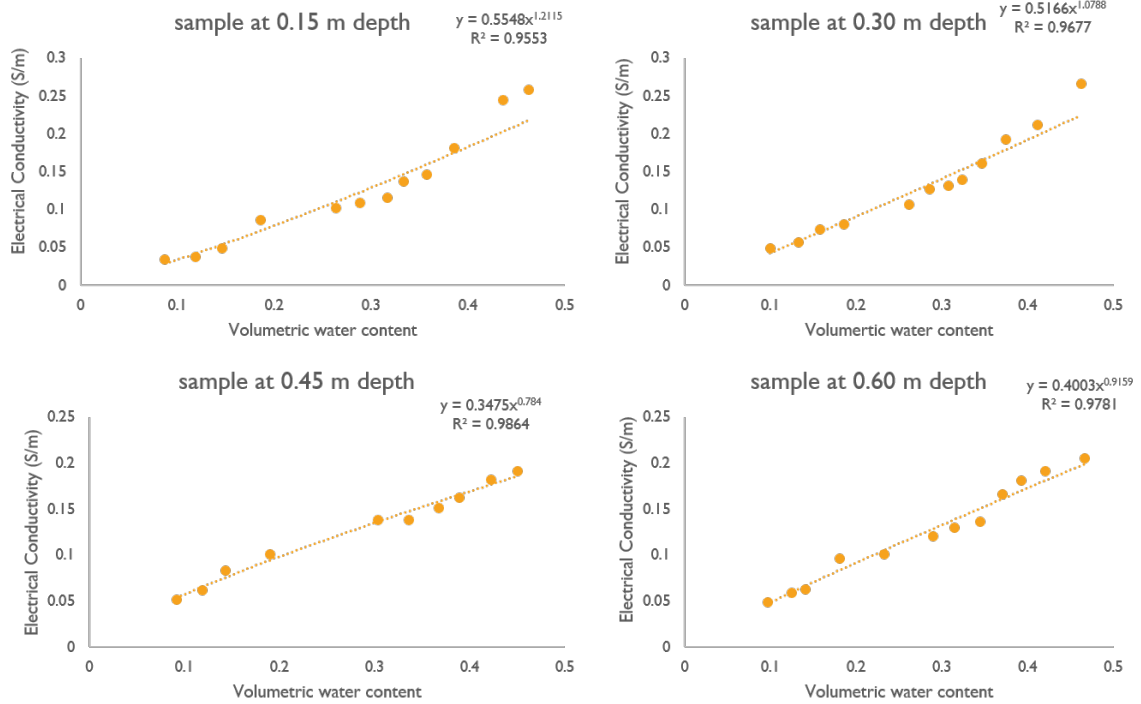| Sample Depth (cm)	'a'	'c'	'b'	RMSE
4-17	0.5548	1.2115	0.005	0.001
17-30	0.5166	1.0788	0.003	0.002
30-43	0.3475	0.7840	0.001	0.001
47-60	0.4003	0.9159	0.003	0.020

Figure 4.6: Electrical Conductivity and soil moisture relationship

trees with same amount of irrigation. The monitoring results for healthy and decline trees were clearly indicating that there is quite different for healthy and decline trees before and after irrigation. Here we will explain one irrigation period results for both healthy and declined trees at same time period.

The initial condition (17.30 IST of 12 March, before Irrigation) for a healthy tree, around the tree show a very clear difference in SWC in the top 30 to 45 cm of the soil with respect to the rest of the volume 4.7. SWC is ranging from 10-20% at top volume, while the lower part of the profile is ranging around 20 to 30% and is following same order of magnitude. At the depth of 40 to 45 cm the soil moisture content divide indicating that no apparent lithological difference present and RWU

plays a role in this portion [22]. After irrigation (9.00 IST of 13 March, irrigation given) at last observation of ERT profile shows that the same order of magnitude of SWC for an entire volume and can't demarcating the RWC potion, because we have applied flood irrigation for an entire grid around the tree. Note that the observation here is that after irrigation the water will be consumed by the tree but we cannot have estimated immediately after irrigation of one to three days, it makes an interest to do numerical simulation which will be discussed last section of this paper. Again note is that after 20 days' observation of ERT profile (9.00 IST of 04 April) the behavior is more or less same as before profile. It may be indicating that immediately after irrigation, it is difficult to observe the RWU distribution which will be consumed by roots in a flood irrigation.

In another case for decline tree the initial condition (16.00 IST of 12 March, before irrigation) around the tree shows same SWC distribution as healthy tree but clearly indicating the depth of dividing zone of RWU is less with respect to the decline tree. In this case the RWU portion was observed at 30 to 35 cm only and may it happen due to less root stock of the disease tree. Note that here we are not considering the level of the decline. The interesting observation noted in decline tree is after irrigation (9.30 IST of 13 March, irrigation given) the SWC distribution was very high and is maintain same magnitude in entire volume of the profile. This results shows that in a decline tree are less capable of taking water after irrigation. Again after 20 days of irrigation the Time-lapse ERT profile indicating the same profile as initial.

4.2.2 Selection of Optimum Root distribution Parameter

Root water uptake parameters are optimized in HYDRUS by one at a time analysis, though it is not exact way to do that but it gives approximately good results. For more accurate results, one can do by using 'PEST' or 'GA and SA' algorithms to optimize root water uptake parameters. Root distribution parameters are z, z^*, r, r^*, P_z, P_r
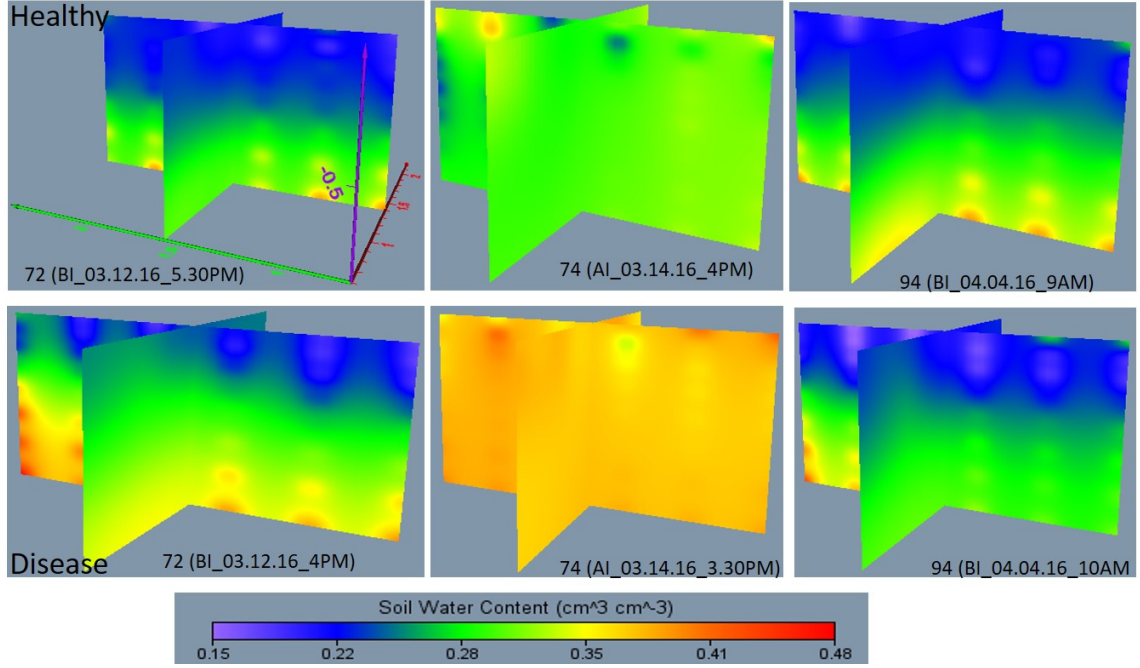
Figure 4.7: Soil Moisture profile for healthy and diseased tree before and after irrigation

which represents maximum depth of root activity, depth at which maximum root uptake is taking place, maximum radius of root activity, radius at which maximum root water uptake is taking place, empirical coefficients in depth and radial direction respectively. We have varied 'z' from 5-70 m, 'z*' from 1-60 m, 'r' from 1-150 m, r* from 1-100 m , P_z&P_z from 0-15. We have changed one parameter keeping other parameter constant and simulated the model. Parameter which resulted in least RMSE value, were assumed as optimal parameter and then by keeping that parameter constant and varying other parameters one by one, all the parameters are optimized. Optimized parameters are given in table 4.3
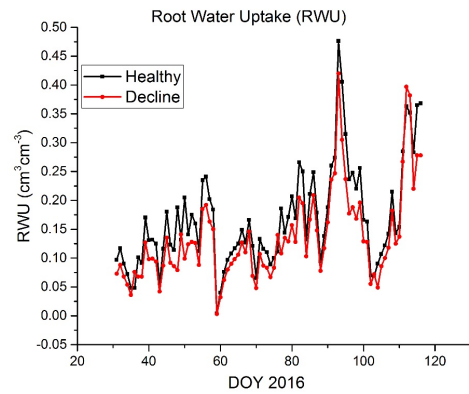
Table 4.3: Root distribution parameters

Type	z	z*	P_z	r	r*	P_r
Healthy	41	32	0.12	168	141	0.21
Diseased	37	23	3.58	161	132	3.39

47

Hydraulic Properties: Theta vs. h
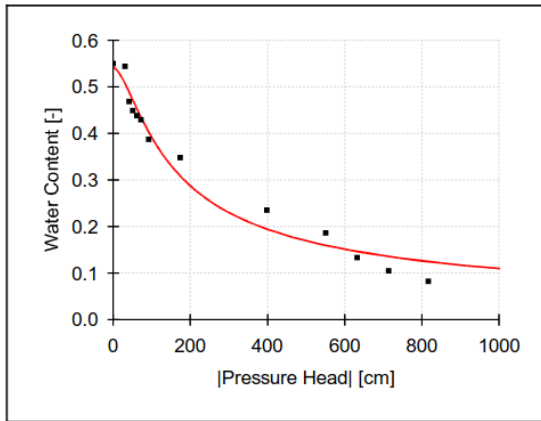
(a) Soil water retention curve

(b) Root water uptake for decline and healthy tree

4.2.3 Root water uptake

Potential transpiration is the major factor in root system to consume water by tree and we feel that it must be different for healthy and decline tree but quantification of transpiration rate is very difficult for each tree and we haven't measured transpiration rate separately for each decline and healthy tree. But to overcome above limitation, we did sensitivity analysis for potential transpiration in the declined tree by decreasing certain percentage from 10 to 50% to the transpiration rate of Healthy tree and for each stage, measured and simulated water contents are compared and it was observed that at 25% decreasing of transpiration shows better agreement for declined tree in this study. The root water uptake distributions for healthy and diseased tree for entire simulation period showed in fig 4.8b. The root water uptake distribution is varying from healthy to decline and observed that slight decreasing of uptake in decline condition.

Chapter 5

Summary and Conclusions

5.1 Summary

In the first part of the study, our objective was to develop open source effective inversion technique for 3D inversion problem. Matlab codes for 3 gradient based algorithm and one compressed sensing algorithm has been developed and tested for synthetic problems. All these algorithm are compared with open source available matlab package 'RESINVM3D' in which inexact Gauss-Newton algorithm has been used. Effective procedure has been derived for explicit calculation of sensitivity matrix. Primal-dual interior point method has been implemented to solve large scale least square problem with l1-norm regularization. Since in 3D ERT inverse problem, model parameters are not sparse so Discrete Cosine Transform has been used for inducing sparsity.

In the second part of the study, our primary objective was to understand soil-water-disease interactions of Citrus trees.For this, time-lapse ERT survey has been

performed for healthy and diseased tree at the same time to get 3D resistivity profile of the root zone. Then resistivity profile were converted into 3D soil moisture profile using Waxman-Smits' model [33]. Then Waxman-Smits' model had been calibrated in the laboratory for samples at four different depths. Then we have developed soil retention curve in the laboratory to get hydraulic parameters using Van-Genuchten model. Root distribution parameters had been optimized using one at a time sensitivity analysis. At the end, water flow has been simulated using axi-symmetric Richard's equation to obtain moisture content in the root zone of Citrus crop and compared with observed moisture content in the field for both healthy and diseased tree. We have observed that root distribution parameter are quite different for both tree and hence we can say that soil-water-plant relationship are different for healthy and diseased tree.

5.2   Conclusions

From this Study we can conclude the following:

1. An open-source MATLAB code was developed for 3-D inversion of ERT data using compressive sensing framework.

2. The developed code was tested on synthetic models with varying degrees of heterogeneity.

3. The CS algorithm is less sensitive to initial uniform model parameters and resulted in quick convergence.

4. A significant improvement in image reconstruction (increase in NRMSE from 0.4670 to 0.7859 from 10 to 5 iterations) was achieved through CS over conventional gradient algorithms.

5. Compressed sensing algorithms performed well when model parameters are very high in comparison to data points.

6. L1-norm regularization used in compressed sensing detected sharp changes in resistivity values.

7. A 3-D ERT protocol was developed and validated for monitoring 3-D soil moisture profiles of healthy and declined matured citrus trees.

8. Both healthy and declined citrus trees have shown different soil moisture distributions in response to irrigation water applied at the surface.

9. A numerical root water uptake (RWU) was developed using Hydrus 2D/3D. Soil-Atmospheric fluxes were provided as per FAO guidelines.

10. Optimal root distribution parameters were derived for both cases (by calibrating simulated soil moisture with ERT data).

11. RWU from a declined tree is far less than that of a healthy tree, with the peak happening in advance (in time domain) resulting from water stress.

5.3 Future Scope

1. 3D time-lapse ERT inversion technique can be developed to detect change in resistivity of the model with time.

2. Inversion results can be validated by exploring the subsurface strata for Compressed sensing.

3. There are scope for development of methodology to induce sparsity for the field condition.

4. Other l1- norm regularized algorithm for large scale least square problems can be applied for inversion.

5. Disease quantification can be done along with soil-water-plant simulation.

6. Quantification of sap flow, transpiration etc. can be done for better results.

7. Specific experimental set-up can be prepared for better control in boundary flows.

5.4   Limitations

1. We have developed static 3D ERT Matlab code which can't detect change in resistivity over time.

2. Analysis has been done on synthetic model and mayn't as accurate in actual field conditions.

3. Discrete Cosine Transformation has been used to induce sparsity in the model but scope of other transformations into ERT inversion problem hadn't explored.

4. Root distribution parameters were different for healthy and diseased tree but the variation of these parameters according to the various level of disease are not determined.

5. Exact amount of transpiration for diseased and healthy tree hasn't be measured.

6. No flow boundary on the lateral direction were assumed where as for some length radial direction, atmospheric condition were assumed and for rest length, variable flux boundary were assumed.

Reference

[1] R. G. Allen, L. S. Pereira, D. Raes, M. Smith et al. Crop evapotranspiration-Guidelines for computing crop water requirements-FAO Irrigation and drainage paper 56. *FAO, Rome* 300, (1998) D05,109.

[2] L. Slichter. The interpretation of the resistivity prospecting method for horizontal structures. *Journal of Applied Physics* 4, (1933) 307–322.

[3] K. Vozoff. Numerical resistivity analysis: horizontal layers. *Geophysics* 23, (1958) 536–556.

[4] A. A. Zohdy, L. Anderson, and L. Muffler. Resistivity, self-potential, and induced-polarization surveys of a vapor-dominated geothermal system. *Geophysics* 38, (1973) 1130–1144.

[5] G. E. Backus and J. Gilbert. Numerical applications of a formalism for geophysical inverse problems. *Geophysical Journal International* 13, (1967) 247–276.

[6] D. D. Jackson. Interpretation of inaccurate, insufficient and inconsistent data. *Geophysical Journal International* 28, (1972) 97–109.

[7] D. D. Jackson. The use of a priori data to resolve non-uniqueness in linear inversion. *Geophysical Journal International* 57, (1979) 137–157.

[8] D. Ghosh. The application of linear filter theory to the direct interpretation of geoelectrical resistivity sounding measurements. *Geophysical prospecting* 19, (1971) 192–217.

[9] V. G. Savita and A. Nagpal. Citrus diseases caused by Phytophthora species. *GERF Bull Biosci* 3, (2012) 18–27.

[10] J. Duniway. Water relations of Fusarium wilt in tomato. *Physiological Plant Pathology* 1, (1971) 537–546.

[11] A. Srivastava, I. Singh, and A. Das. Citrus production constraints in Meghalaya: issues and strategies. *Himalayan Ecol* 18, (2011) 14–24.

[12] G. Jagtap, M. Dhavale, and U. Dey. Evaluation of natural plant extracts, antagonists and fungicides in controlling root rot, collar rot, fruit (brown) rot and gummosis of citrus caused by Phytophthora spp. in vitro. *Scientific Journal of Microbiology* 1, (2012) 27–47.

[13] J. Graham and E. Feichtenberger. Citrus Phytophthora diseases: management challenges and successes. *Journal of Citrus Pathology* 2.

[14] R. Gade et al. Biological and chemical management of Phytophthora root rot/collar rot in citrus nursery. *The Bioscan* 7, (2012) 631–635.

[15] Y. Levy, R. Levi, and Y. Cohen. Buildup of a pathogen subpopulation resistant to a systemic fungicide under various control strategies: A flexible simulation model. *Phytopathology* 73, (1983) 1475–1480.

[16] T. Kean and M. Thanou. Biodegradation, biodistribution and toxicity of chitosan. *Advanced drug delivery reviews* 62, (2010) 3–11.

[17] S. J. Olsen, L. MacKinnon, J. S. Goulding, N. H. Bean, L. Slutsker et al. Surveillance for foodborne-disease outbreaksUnited States, 1993–1997. *MMwR CDC Surveill Summ* 49, (2000) 1–62.

[18] D. B. Bright, J. H. Graham, M. S. Irey, and L. E. Baucum. Soil, rootstock and climatic factors affect populations of Phytophthora nicotianae in south Florida citrus plantings. In Proceedings of the Florida State Horticultural Society, volume 117. 2004 148–151.

[19] M. A. Meju. Geophysical data analysis: Understanding inverse problem theory and practice, volume 6. Society of Exploration Geophysicists Tulsa,, OK, 1994.

[20] A. Pidlisecky and R. Knight. FW2_5D: A MATLAB 2.5-D electrical resistivity modeling code. *Computers & Geosciences* 34, (2008) 1645–1654.

[21] E. Haber. Numerical strategies for the solution of inverse problems. Ph.D. thesis, University of British Columbia 1997.

[22] G. Cassiani, J. Boaga, D. Vanella, M. T. Perri, and S. Consoli. Monitoring and modelling of soil–plant interactions: the joint use of ERT, sap flow and eddy covariance data to characterize the volume of an orange tree root zone. *Hydrology and Earth System Sciences* 19, (2015) 2213–2225.

[23] S. Whitaker. Flow in porous media I: A theoretical derivation of Darcy's law. *Transport in porous media* 1, (1986) 3–25.

[24] J. P. Walker, G. R. Willgoose, and J. D. Kalma. In situ measurement of soil moisture: a comparison of techniques. *Journal of Hydrology* 293, (2004) 85–99.

[25] I. Srayeddin and C. Doussan. Estimation of the spatial variability of root water uptake of maize and sorghum at the field scale by electrical resistivity tomography. *Plant and Soil* 319, (2009) 185–207.

[26] S. Garré, M. Javaux, J. Vanderborght, H. Vereecken et al. Three-dimensional electrical resistivity tomography to monitor root zone water dynamics. *Vadose Zone Journal* 10, (2011) 412–424.

[27] U. Werban, S. Attia al Hagrey, and W. Rabbel. Monitoring of root-zone water content in the laboratory by 2D geoelectrical tomography. *Journal of Plant Nutrition and Soil Science* 171, (2008) 927–935.

[28] J. Boaga, M. Rossi, and G. Cassiani. Monitoring soil-plant interactions in an apple orchard using 3D electrical resistivity tomography. *Procedia Environmental Sciences* 19, (2013) 394–402.

[29] L. Beff, T. Günther, B. Vandoorne, V. Couvreur, and M. Javaux. Three-dimensional monitoring of soil water content in a maize field using Electrical Resistivity Tomography. *Hydrology and Earth System Sciences* 17, (2013) 595–609.

[30] B. F. Schwartz, M. E. Schreiber, and T. Yan. Quantifying field-scale soil moisture using electrical resistivity imaging. *Journal of Hydrology* 362, (2008) 234–246.

[31] P. Brunet, R. Clément, and C. Bouvier. Monitoring soil water content and deficit using Electrical Resistivity Tomography (ERT)–A case study in the Cevennes area, France. *Journal of Hydrology* 380, (2010) 146–153.

[32] M. T. Van Genuchten. A closed-form equation for predicting the hydraulic conductivity of unsaturated soils. *Soil science society of America journal* 44, (1980) 892–898.

[33] M. Waxman, L. Smits et al. Electrical conductivities in oil-bearing shaly sands. *Society of Petroleum Engineers Journal* 8, (1968) 107–122.

[34] S. Reynolds. The gravimetric method of soil moisture determination Part III An examination of factors influencing soil moisture variability. *Journal of Hydrology* 11, (1970) 288–300.

[35] J. Simunek and M. Sejna. HYDRUS technical manual, version 2. PC-Progress, 2011.

[36] J. Simunek, M. Sejna, and M. van Genuchten. The HYDRUS-1D software package for simulating the one-dimensional .

[37] R. Feddes and P. Raats. Parameterizing the soil–water–plant root system. *Unsaturated-zone modeling: Progress, challenges, and applications. Wageningen UR Frontis Ser* 6, (2004) 95–141.

[38] J. Vrugt, M. v. Wijk, J. W. Hopmans, and J. Šimunek. One-, two-, and three-dimensional root water uptake functions for transient modeling. *Water Resources Research* 37, (2001) 2457–2470.

[39] V. Phogat, M. Skewes, J. Cox, J. Alam, G. Grigson, and J. Šimunek. Evaluation of water movement and nitrate dynamics in a lysimeter planted with an orange tree. *Agricultural water management* 127, (2013) 74–84.